

Generalization properties of restricted Boltzmann machine for short-range order

M A Timirgazin and A K Arzhnikov

Citation: Chin. Phys. B, 2023, 32 (**6**): 067401. DOI: 10.1088/1674-1056/ac989c
Journal homepage: http://cpb.iphy.ac.cn; http://iopscience.iop.org/cpb

What follows is a list of articles you may be interested in

Learnable three-dimensional Gabor convolutional network with global affinity attention for hyperspectral image classification

Hai-Zhu Pan(潘海珠), Mo-Qi Liu(刘沫岐), Hai-Miao Ge(葛海淼), and Qi Yuan(袁琪)
Chin. Phys. B, 2022, 31 (**12**): 120701. DOI: 10.1088/1674-1056/ac8cd7

Ionospheric vertical total electron content prediction model in low-latitude regions based on long short-term memory neural network

Tong-Bao Zhang(张同宝), Hui-Jian Liang(梁慧剑),Shi-Guang Wang(王时光), and Chen-Guang Ouyang(欧阳晨光)
Chin. Phys. B, 2022, 31 (**8**): 080701. DOI: 10.1088/1674-1056/ac4487

Memristor-based multi-synaptic spiking neuron circuit for spiking neural network

Wenwu Jiang(蒋文武), Jie Li(李杰), Hongbo Liu(刘洪波), Xicong Qian(钱曦聪), Yuan Ge(葛源), Lidan Wang(王丽丹), and Shukai Duan(段书凯)
Chin. Phys. B, 2022, 31 (**4**): 040702. DOI: 10.1088/1674-1056/ac380b

Effects of pressure and/or magnetism on superconductivity of δ-MoN single crystal

Miao Bo-Tong (苗博童), Wang Shan-Min (王善民), Kong Pan-Pan (孔盼盼), Jin Mei-Ling (金美玲), Feng Shao-Min (冯少敏), Zhang Si-Jia (张思佳), Hao Ai-Min (郝爱民), Yu Xiao-Hui (于晓辉), Jin Chang-Qing (靳常青), Zhao Yu-Sheng (赵予生)
Chin. Phys. B, 2015, 24 (**1**): 017403. DOI: 10.1088/1674-1056/24/1/017403

Magnetic property improvement of niobium doped with rare earth elements

Jiang Tao (江涛), He Fei-Si (贺斐思), Jiao Fei (焦飞), He Fa (何法), Lu Xiang-Yang (鲁向阳), Zhao Kui (赵夔), Zhao Hong-Yun (赵红运), You Yu-Song (游雨松), Chen Lin (陈林)
Chin. Phys. B, 2014, 23 (**5**): 057403. DOI: 10.1088/1674-1056/23/5/057403

Generalization properties of restricted Boltzmann machine for short-range order

M A Timirgazin[†] and A K Arzhnikov

Udmurt Federal Research Center, Ural Branch of RAS, Izhevsk 426067, *Russia*

(Received 27 July 2022; revised manuscript received 20 September 2022; accepted manuscript online 10 October 2022)

A biased sampling algorithm for the restricted Boltzmann machine (RBM) is proposed, which allows generating configurations with a conserved quantity. To validate the method, a study of the short-range order in binary alloys with positive and negative exchange interactions is carried out. The network is trained on the data collected by Monte–Carlo simulations for a simple Ising-like binary alloy model and used to calculate the Warren–Cowley short-range order parameter and other thermodynamic properties. We demonstrate that the proposed method allows us not only to correctly reproduce the order parameters for the alloy concentration at which the network was trained, but can also predict them for any other concentrations.

Keywords: machine learning, short-range order, Ising model, restricted Boltzmann machine

PACS: 74.70.Ad, 07.05.Mh, 64.60.De **DOI:** 10.1088/1674-1056/ac989c

1. Introduction

The use of machine learning (ML) methods has proved its efficiency in various technical devices. Neural networks have made a breakthrough in speech and image recognition technologies, the implementation of control of complex technical devices and manufacturing processes. In recent years, ML has grown in popularity as a powerful scientific tool. Neural networks are used for identification and classification of phases in classical and quantum systems,[1–7] accelerating molecular dynamics[8,9] and Monte–Carlo simulations,[10–12] generating the conformational properties of a polymers[13] and many other fields (see the reviews[14,15]).

Among the various architectures of neural networks, of particular interest is the restricted Boltzmann machine (RBM), a simple generative energy-based model.[16] The main feature of RBM is the hidden layer, which in physical language can be interpreted as an introduced auxiliary field allowing you to decouple complex interaction between visible variables. This is similar to the Hubbard–Stratonovich transformation.[17] As calculations of Ising-like systems show (see, for example, Ref. [18]) the self-consistent field distribution has two Gaussian peaks that can be interpreted as hidden variables taking the values $+1$ or -1 with certain amplitudes. The RBM structure well reflects the above fact and its training is analogous to the search for field distribution amplitudes that best reproduce the training data, thereby minimizing the free energy.[19]

Based on principles of statistical mechanics, RBM turns out to be able to capture the physics underlying classical and quantum many-body problems.[19–22] It is important that RBM can not only classify and process large data, but can be used even for reconstructing the ground state wave function.[23] While RBM is usually treated as a component of deep belief networks,[24] it is found that at least for Ising model the shallow RBM gives just as good results as deep models being much more simple in training.[25]

A recent study[26] found limitations in the RBM application to the systems with a conserved quantity. The authors trained RBM on a data set obtained from Monte–Carlo simulations for the two-dimensional Ising model with conserved magnetization. Configurations generated by the machine had forbidden magnetization and energy values. In the present work, a binary alloy is considered that can be described by the Ising model with conserved magnetization. We develop an algorithm for how RBM can generate samples with a fixed concentration (magnetization), which helps to overcome the disadvantage indicated in Ref. [26].

We train RBM on data sets obtained from Monte–Carlo simulations for the ferromagnetic and antiferromagnetic binary systems with the short-range order. Applying the proposed biased sampling algorithm, we show that the generated configurations by RBM have the correct order parameters. Moreover, we found that it is possible to sample configurations with any given concentration, and not just the one on which training is performed. This demonstrates generalization properties of RBM and have great potential for possible practical applications.

2. Model

2.1. Short-range order

Short-range order (SRO) refers to the regular and predictable arrangement on a local length scale. A simple system with SRO is a binary alloy of A and B components (Fig. 1), the

[†]Corresponding author. E-mail: timirgazin@gmail.com

© 2023 Chinese Physical Society and IOP Publishing Ltd

energy of which can be written as a sum of pair potentials[27]

$$E = N_{AA}\phi_{AA} + N_{BB}\phi_{BB} + N_{AB}\phi_{AB}, \tag{1}$$

where $N_{\alpha\beta}$ is the number of atom pairs α and β, and $\phi_{\alpha\beta}$ is their energy. Let us introduce a quasi-spin S_i that takes the value $+1$ or -1 if the site i occupied by an atom A or B, respectively. Then the energy of the system (1) can be represented in the Ising-like form[27]

$$\mathcal{H} = -J\sum_{\langle i,j\rangle} S_i S_j - h\sum_i S_i + C_0, \tag{2}$$

where $J = \frac{1}{2}[\phi_{AB} - \frac{1}{2}(\phi_{AA} + \phi_{BB})]$, $h = \frac{1}{4}z(\phi_{BB} - \phi_{AA})$, $C_0 = \frac{1}{4}zN(\frac{1}{2}\phi_{AA} + \frac{1}{2}\phi_{BB} + \phi_{AB})$, N is the total number of sites, and z is the coordination number. The constant and external-field terms can be omitted under the assumption $\phi_{AA} = \phi_{BB}$:

$$\mathcal{H} = -J\sum_{\langle i,j\rangle} S_i S_j. \tag{3}$$

The same components tend to cluster together if $J > 0$ (ferromagnetic order), form unlike pairs if $J < 0$ (antiferromagnetic order), and are perfectly disordered in the case of $J = 0$. Despite its simplicity, in the high temperature regime the Ising model allows both qualitative and quantitative description of various orderings and phase transitions in binary systems.[28–30]

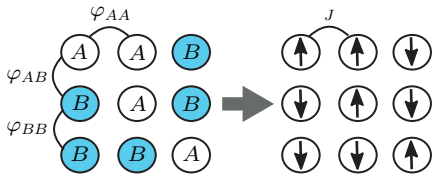


Fig. 1. Transformation of binary (A and B) alloy problem to Ising spin model on square lattice.

SRO is most commonly described by the Warren–Cowley (WC) parameter,[31,32] which is the pair-correlation function

$$\alpha = 1 - \frac{P_{AB}}{x}, \tag{4}$$

where P_{AB} is the probability of a B atom being found at a site nearest to the A atom, and x is the concentration of A atoms. The sign of WC parameter coincides with the sign of interaction parameter J, with $\alpha = 0$ corresponding to perfect disorder.

2.2. Monte–Carlo simulation

Similarity with the Ising model suggests that SRO of a finite system can be effectively studied by Monte–Carlo (MC) simulation.[33] There are following differences from the common Metropolis–Hastings algorithm for the magnetic Ising model:[34] the alloy concentration (net magnetization in terms of magnetism) is set at the system initialization and remains fixed during simulation, and not a spin-flip on site, but a change from AB to BA bond is made at every MC step.

We consider the system of $N = L \times L$ sites with $L = 10$ and periodic boundary conditions. We start with a random distribution of atoms (spins) with the required concentration. The concentrations considered are in the range from 0.05 to 0.95 with a step of 0.05. Each trial to change the neighboring atoms A and B (spins $\uparrow$ and $\downarrow$) is accepted according to the Metropolis prescription (Kawasaki algorithm[35]). To reach the equilibrium state we take 10^3 MC steps for all the concentrations studied, where one MC step consists of N spin-exchange attempts. This is more than N MC steps that are usually taken for the Metropolis–Hastings algorithm, because we assume that the acceptance ratio for Kawasaki algorithm can be smaller. Then, we take 10^7 MC steps to collect the data set $\mathcal{D}$ of 10^5 samples over which averaging will occur. The large size of the data set allows us to avoid overfitting problem and use regularization in the further training of the neural network.[20]

In the ferromagnetic (FM) case, the system manifests long-range order at any $J > 0$ because holding the concentration acts like an external field and implies the absence of phase transition. At the same time, at $J > J_c$ the system undergoes phase separation.[36] The case of antiferromagnetic (AFM) interaction is much more complex: the model undergoes a phase transition from the ordered AFM to disordered paramagnetic (PM) state even in the presence of an external field.[37] There is no exact analytical results for the critical values and numerical simulations are also problematic.[37,38]

We restrict ourselves by the consideration of FM $J = +0.2$ and AFM $J = -0.2$ interactions (it is assumed that the temperature $T = 1$). The magnitude of J is chosen to stay in the single-phase region and to ensure that in the case of AFM interaction the system is in PM state far from phase transition for any alloy concentration. So we avoid problems with phase separation and AFM LRO, and at the same time can study two essentially different cases with the standard Metropolis MC algorithm on a relatively small lattice. Omitting the possibility of phase separation does not significantly limit the applicability of our approach, because many real alloys with short-range order have broad single-phase concentration ranges (see, e.g., Refs. [29,39]), and the basic concept of the novel high-entropy alloys requires a single-phase state.[40,41] The case of phase separation needs a more detailed consideration (as it was done for non-ergodic systems in Ref. [7]).

For both the FM and AFM cases, we run MC simulations and collect data sets $\mathcal{D}$, over which averaging is performed. Figure 2 shows some random samples from data sets $\mathcal{D}$ for $x = 0.5$ with $J = +0.2$ and $J = -0.2$. It can be clearly seen how the atoms of the same type tend to cluster together for positive J and how the atoms of different types tend to occupy neighboring sites for negative J. The calculated average WC parameters $\langle\alpha\rangle$ reach their extreme values at $x = 0.5$ and tend

to zero at boundaries because SRO is meaningless when all of the atoms are equal.

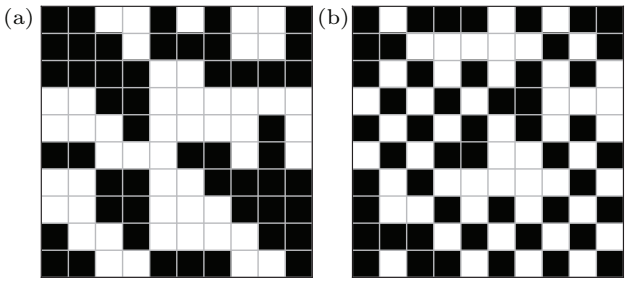


Fig. 2. Examples of atoms distribution obtained by MC simulations for $J = +0.2$ (a) and $J = -0.2$ (b).

2.3. Restricted Boltzmann machine

The full Boltzmann machine, a stochastic energy-based neural network, consists of two types of neurons (nodes): visible and hidden.[16] Each node is binary and connected to other nodes with some weight. If the connections between neurons of the same type are forbidden, the model is called the restricted Boltzmann machine.[42] The architecture of RBM is depicted in Fig. 3: all neurons are arranged in visible ($i = 1,\ldots,n$) and hidden ($j = 1,\ldots,m$) layers interconnected with weights $w_{i,j}$. Together with biases a_i and b_j, the weights constitute the RBM parameter set denoted by θ. These parameters determine the energy of a given configuration (v,h):

$$E(v,h) = -\sum_i a_i v_i - \sum_j b_j h_j - \sum_{i,j} v_i w_{i,j} h_j. \tag{5}$$

The probability distribution over hidden and visible vectors is defined by Boltzmann distribution

$$P(v,h) = \frac{1}{Z} \mathrm{e}^{-E(v,h)}, \tag{6}$$

where Z has the meaning of the partition function.

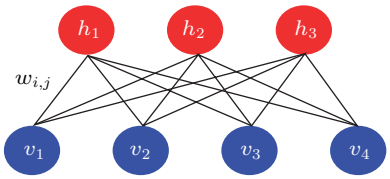


Fig. 3. Boltzmann machine architecture.

RBMs gained wide popularity in the 2000s, because some efficient training algorithms were developed by Hinton.[43] Once RBM is trained, which means that the parameter set θ is found, a new data set $\mathcal{S}$ can be generated by the block Gibbs sampling procedure. Successful training provides similarity between the real physical probability distribution and the probability distribution of the generated data set. The method of RBM training is described in detail in Ref. [44]. The main idea is to use the so-called contrastive divergence approximation with k steps (CD-k) to perform stochastic gradient descent procedure for the negative log-likelihood function. Contrastive divergence procedure becomes possible due to bipartite structure of RBM, which enables the block Gibbs sampling. The hidden layer can be completely obtained from the known visible layer, and vice versa, by the conditional probabilities

$$p(h_j = 1|v) = \sigma\left(b_j + \sum_i w_{i,j} v_i\right), \tag{7}$$

$$p(v_i = 1|h) = \sigma\left(a_i + \sum_j w_{i,j} h_j\right). \tag{8}$$

To generate a new data set by trained RBM, one can initialize visible layer by random values v_0 and run Gibbs sampling procedure, i.e., to compute hidden layer h_0, then new visible layer v_1, and then new hidden layer h_1 and so on. After some equilibration period (like in usual MC method) the generated visible units can be collected to the data set $\mathcal{S}$, which is expected to obey the same probability distribution as the data set $\mathcal{D}$. Averaging over $\mathcal{S}$ allows to calculate the observable physical values like mean energy or heat capacity.

3. Results

In order to produce the training data set $\mathcal{D}$, we use the standard Markov chain MC technique described in Section 2. The importance sampling yields 10^5 independent spin configurations for $J = +0.2$ and $J = -0.2$ for each concentration $x \in [0.05; 0.95]$ in steps of $\Delta x = 0.05$.

Preliminary examinations have given us the following optimal RBM parameters, which are used further for training: the number of hidden units is equal to the number of visible units $n_h = n_v = 100$, contrastive divergence with the only one step (CD-1), learning rate $\eta = 0.01$, minibatch size 100, and the number of learning epochs 1000 (definitions of training parameters can be found in Appendix A). RBMs with these parameters are trained on data set $\mathcal{D}$ at each concentration of the studied range. In order to illustrate the learning process, we present typical graph of decreasing reconstruction error (mean square deviation between original and reconstructed data[44]) and increasing pseudo-likelihood (approximated value of the likelihood function[45]) during training (Fig. 4).

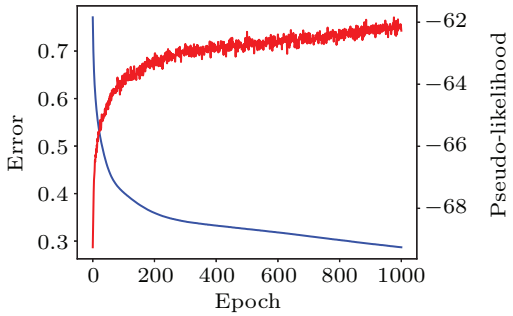


Fig. 4. Monitoring the RBM training process. Reconstruction error (blue) and pseudo-likelihood (red).

At the first stage, we address the question how well can RBM reproduce the observable physical quantities known from MC simulations. In order to answer it, we generate a new data set $\mathcal{S}$ of 10^5 samples at each concentration by the corresponding RBMs and calculate the average observables. 100 Gibbs steps were used to reach the equilibrium state and then the samples were recorded in $\mathcal{S}$ every 50 steps. In Figs. 5–7, computed by such a way, energy $\langle E\rangle$, WC parameter $\langle\alpha\rangle$ and heat capacity $\langle C\rangle = \left(\langle E^2\rangle - \langle E\rangle^2\right)/T^2$ are depicted as 'straight RBM' and compared with the 'exact' values obtained by MC simulations for FM interaction. While the WC parameter and the energy show good agreement, the heat capacity is not satisfactory at all. This is explained by strong sensitivity of long-range correlations to the alloy concentration which is actually is variable in each data set. The reason is that the Gibbs sampling scheme being fundamentally stochastic procedure gives the concentration x_0 (at which RBM was trained) only on average, but the concentrations of each individual sample of $\mathcal{S}$ is fluctuating around x_0. These fluctuations result in fluctuations of the heat capacity.

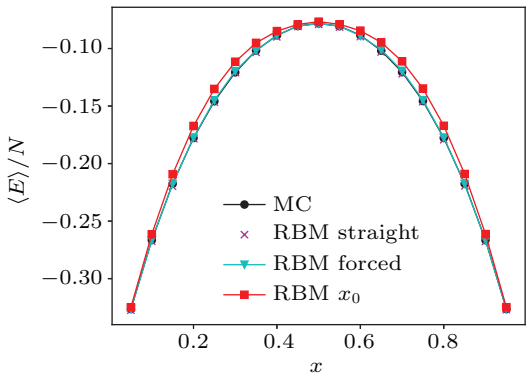


Fig. 5. Energy per site for FM interaction. Black solid line denotes MC simulation, cross markers are straight RBM, cyan triangles are forced RBM, red squares are RBM trained on $x_0 = 0.5$ data set.

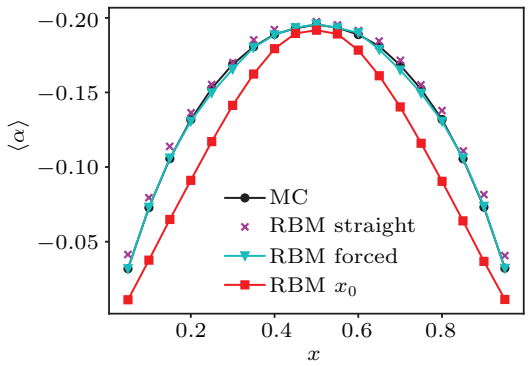


Fig. 6. Warren–Cowley parameter for FM interaction. Black solid line denotes MC simulation, cross markers are straight RBM, cyan triangles are forced RBM, red squares are RBM trained on $x_0 = 0.5$ data set.

The inability to reproduce configurations in presence of a conserved magnetization (concentration) was noted in the recent study.[26] The authors imposed a zero magnetization constraint, which corresponds to $x = 0.5$ in our notation, and stated that RBM is incapable of generating samples with a given magnetization at any temperature. To solve this problem, we propose a sampling algorithm for forcing the concentration to have the required value x_0. A flowchart of the algorithm is depicted in Fig. 8. For every time a new configuration (visible layer) is generated, its concentration is calculated immediately. If the concentration is equal to the required x_0, we accept this sample. If the concentration is lower than x_0, we need to reduce the number of excess B atoms. To do this, we choose a random node k of type B and re-make its binarization by comparing $p(v_k = 1|h)$ (8) with a random number from 0 to 1. If the atom type changes but the concentration is still not equal to x_0, we repeat the procedure of random atom selection and re-binarization until the required concentration x_0 is reached. Similar steps are taken in the case of $x > x_0$. Finally, we record the layer with the concentration x_0 in the dataset. So we achieve that all the samples have the same concentration x_0. Averaging over the data sampled by RBM with the described forcing procedure gives the values presented as 'RBM forced' in Figs. 5–7 for FM interaction and Figs. 9–11 for AFM interaction. As can be seen all the observables now agree much better with MC data. It should be noted that not only the average values coincide, but also the variances. For example, for $x = 0.5$ in the FM case, the variance $\sigma^2 = 0.0056$ and differs between MC and RBM by 0.5%.

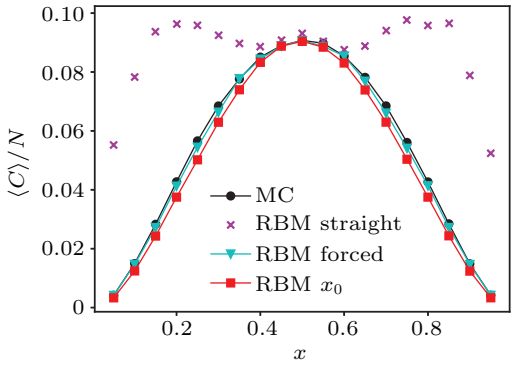


Fig. 7. Heat capacity per site for FM interaction. Black solid line denotes MC simulation, cross markers are straight RBM, cyan triangles are forced RBM, red squares are RBM trained on $x_0 = 0.5$ data set.

The goal of the second stage of our research is to check whether it is possible to access the information about SRO at some arbitrary concentration by RBM trained at completely different concentration. In order to do it one should have a possibility to generate samples with arbitrary concentration. We assumed that the algorithm described by flowchart (Fig. 8) can be applied to solve this problem. Indeed, this procedure does not contain any restrictions for the concentration x_0: stochastic nature of RBM allows for forcing any concentration x' in sample with a sufficient number of repetitions of the flowchart steps. The only limitation is that in the case of an excessively large difference between the desirable concentration x' and the

concentration of the training data set x_0 ($\Delta x = x' - x_0$), the average value of the probabilities (8) will be so far from x' that a very large number of iterations of the scheme (Fig. 8) will be required to achieve it. To make it easier to achieve the required concentration, we modify the probability definition (8) as follows: $p(v_i = 1|h) = \min\left(\sigma(a_i + \sum_j w_{i,j}h_j) + \Delta x, 1\right)$. Adding Δx to the probabilities allows us to shift the average concentration in a sample generated by RBM to the side of x'. This trick helps us to get already at the first iteration of the scheme (Fig. 8) a concentration close to x'. It should be noted that this step is not mandatory for the operation of our algorithm and is just one of the possible ways to speed up the computation. As a result we have an efficient and fast method to force the alloy concentration in the generated data set $\mathcal{S}$ to have an arbitrary value.

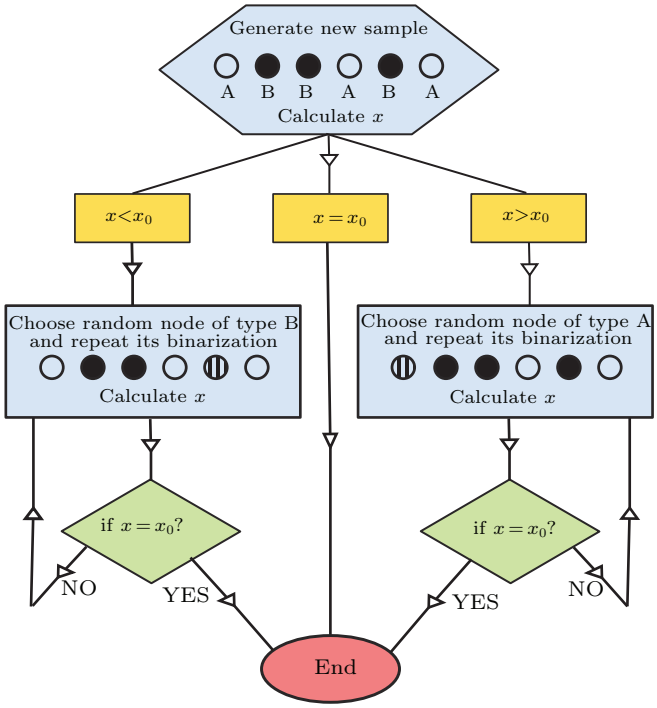


Fig. 8. Flowchart of the sample generation with the forced concentration x_0.

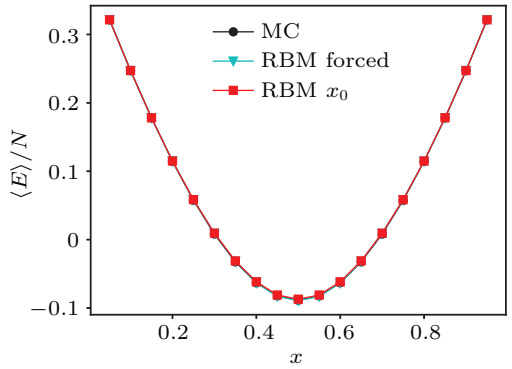


Fig. 9. Energy per site for AFM interaction. Black solid line denotes MC simulation, cyan triangles are forced RBM, red squares are RBM trained on $x_0 = 0.5$ data set.

With the help of the described algorithm, we use RBM trained at $x_0 = 0.5$ to generate data for all the concentrations from 0 to 1 with the step 0.05. 10^5 samples are prepared for each concentration and the average observables are computed. The results are presented as 'RBM x_0' in Figs. 5–7 for FM interaction and in Figs. 9–11 for AFM interaction. A comparison with the 'exact' MC data leads to an impressive conclusion: RBM trained at one concentration satisfactorily reproduces both qualitative and quantitative character of SRO and other observables at any concentration, including those far from original x_0.

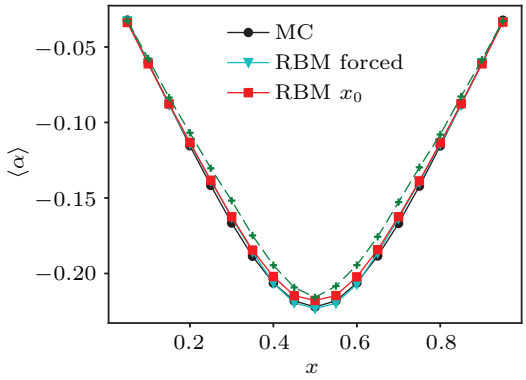


Fig. 10. Warren–Cowley parameter for AFM interaction. Black solid line denotes MC simulation, cyan triangles are forced RBM, red squares are RBM trained on $x_0 = 0.5$ data set. Green dashed line is calculated by RBM trained on reduced data set.

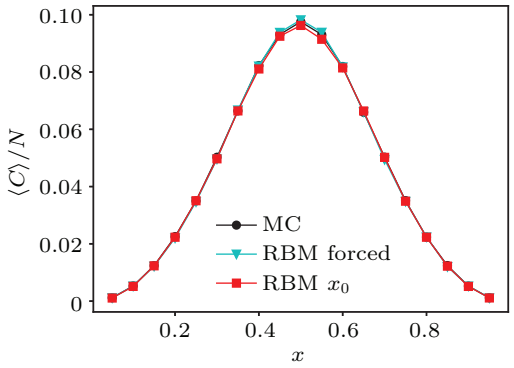


Fig. 11. Heat capacity per site for AFM interaction. Black solid line denotes MC simulation, cyan triangles are forced RBM, red squares are RBM trained on $x_0 = 0.5$ data set.

It is important to note that the conclusions obtained are stable in relation to changes in the training parameters. In particular, reducing the training data set ($\mathcal{D}$ of 10^5 configurations is needed to accurately calculate the observables, but is probably redundant for training), preserves the predictive power of RBM. The WC parameter calculated with a machine trained at a concentration of $x_0 = 0.5$ on a data set of 10^3 samples for the AFM case is shown in Fig. 10 by dashed line. It can be seen that it still agrees well with the exact data.

The reason why RBM trained at one concentration can be used to calculate the order parameters at a different concentration can be explained as follows. Regardless of the total concentration, each sample has local areas where the local concentration may differ. If the dataset is large enough, then

it will contain local ordering patterns of all possible concentrations. By applying RBM to an alloy with a concentration different from the original one, we just artificially (by biased sampling) increase the number of patterns characteristic of a given concentration, while reducing the number of other patterns.

4. Conclusions

Previously it was shown that RBM fails when applied to systems with a conserved magnetization.[26] This shortcoming was expected to manifest itself in other systems as well, which would be a serious limitation in the use of RBM as a tool for physical research. In this study, we found a way to solve this problem by modifying the sampling scheme so that within it the magnetization was strictly fixed. Using this method, we calculated the values of the short-range order parameter, energy, and heat capacity for a binary alloy system and showed that they coincide with the values obtained in MC simulations.

We demonstrated the predictive power of generative neural networks for the systems exhibiting short-range order. The algorithm is proposed that allows using a machine trained on some alloy concentration to calculate the order parameters at any other alloy concentration. Compared to the regular Metropolis–Hastings algorithm, in which MC trials for each site are performed strictly sequentially, Gibbs sampling, thanks to the RBM architecture, allows sampling all the nodes simultaneously, which is much more efficient and opens the way to parallel computations.

Applicability of our algorithm appears to be remarkably wide. It is suitable for the prediction of the SRO and thermodynamic properties in the cases of positive and negative effective interactions, the ordered and disordered phases, close and far from the original concentration. This may be explained by the inherent ability of the neural networks to recognize the patterns underlying the data, combined with an exceptional ability of RBM, as a stochastic generative network, to reproduce these patterns in the sampled data in a controlled manner.

The proposed method is approved for the two-component system but can be naturally extended to the case of multicomponent alloys (RBM extension to non-binary units is considered in Ref. [44]). This can be particularly useful in the context of the high-entropy alloys investigation, novel materials with exceptional mechanical properties. They are consisted of five or more elements and their characteristics are very sensitive to local chemical environment. Monte–Carlo simulations for such systems (see, e.g., Ref. [46]) are very expensive in terms of computational time and the search for the optimal composition by trying all possible concentrations is problematic. RBM trained on some samples taken from MC simulations would shed light on inaccessible areas of concentration, spending relatively little computing resources.

Another promising application is to find a local atomic environment in alloys based on experimental data for a single concentration. For example, if we have the probabilities of the clusters with different atomic configurations from the experiment, we can use MC approach to generate a data set where each sample is ordered accordingly. Using our algorithm, we can train RBM on this data set and predict the local atomic configurations, and hence the other properties, e.g., hyperfine field or local magnetization,[29] for the concentrations other than the experimental one.

Appendix: RBM training

Unsupervised RBM training implies learning an unknown distribution $P(v)$ based on sample data. Specifically for RBM it means adjusting the parameters $\theta = \{w_{i,j}, a_i, b_j\}$ of the probability distribution $P(v|\theta)$ that maximize the likelihood of the training data set $\mathcal{D} = \{v_1, \ldots, v_n\}$. Maximizing the likelihood $\mathcal{L}(\theta|\mathcal{D})$ corresponds to minimizing the distance between the unknown distribution P_{data} underlying $\mathcal{D}$ and the model distribution P_{model} in terms of the Kullback–Leibler divergence (KL divergence), which is given by

$$\mathrm{KL}(P_{\text{data}}||P_{\text{model}}) = \sum_i P_{\text{data}}(v_i) \ln P_{\text{data}}(v_i) - \sum_i P_{\text{model}}(v_i) \ln P_{\text{model}}(v_i). \tag{A1}$$

Differentiating this we can solve the optimization problem and deduce an update rules for the gradient ascent on the log-likelihood:[43]

$$w_{i,j}^{(t+1)} = w_{i,j}^{(t)} + \eta \left(\langle v_i h_j \rangle_{\text{data}} - \langle v_i h_j \rangle_{\text{model}} \right), \tag{A2}$$

$$a_i^{(t+1)} = a_i^{(t)} + \eta \left(\langle v_i \rangle_{\text{data}} - \langle v_i \rangle_{\text{model}} \right), \tag{A3}$$

$$b_j^{(t+1)} = b_j^{(t)} + \eta \left(\langle h_j \rangle_{\text{data}} - \langle h_j \rangle_{\text{model}} \right), \tag{A4}$$

where η is the learning rate.

Average $\langle \cdots \rangle_{\text{model}}$ values can be obtained by Gibbs sampling chain

$$v^0 \to h^0 \to v^1 \to h^1 \to \cdots \to v^k \to h^k \tag{A5}$$

by using conditional probabilities (7) and (8) until the stationary distribution is reached. The idea of RBM training is to limit the chain (A5) to a few k-steps, which turned out to be sufficient for effective learning. This is so called contrastive divergence (CD-k) method, and in practice $k = 1$ is usually used.[43] Then the update rules look like

$$w_{i,j}^{(t+1)} = w_{i,j}^{(t)} + \eta \left(v_i^0 h_j^0 - v_i^1 h_j^1 \right). \tag{A6}$$

To speed up the training procedure, the data set $\mathcal{D}$ is split into minibatches of small size and the update of weights and biases is done after each minibatch and not after the entire set.

Starting from zero biases a_i, b_j and random weights $w_{i,j}$ normally distributed around zero, we run an iterative procedure, each step of which corresponds to one learning epoch. The above algorithm is the standard way for RBM training and has proven to be effective in numerous applications.

Acknowledgement

This study was supported by the financing program AAAA-A16-116021010082-8.

References

[1] Wang L 2016 *Phys. Rev. B* **94** 195105
[2] Carrasquilla J and Melko R G 2017 *Nat. Phys.* **13** 431
[3] Hu W, Singh R R P and Scalettar R T 2017 *Phys. Rev. E* **95** 062122
[4] Shiina K, Mori H, Okabe Y and Lee H K 2020 *Scientific Reports* **10** 2177
[5] Wetzel S J 2017 *Phys. Rev. E* **96** 022140
[6] Ch'ng K, Carrasquilla J, Melko R G and Khatami E 2017 *Phys. Rev. X* **7** 031038
[7] Westerhout T, Astrakhantsev N, Tikhonov K S, Katsnelson M I and Bagrov A 2020 *Nat. Commun.* **11** 1593
[8] Noé F, Tkatchenko A, Müller K R and Clementi C 2020 *Annual Review of Physical Chemistry* **71** 361
[9] Smith J S, Isayev O and Roitberg A E 2017 *Chem. Sci.* **8** 3192
[10] Liu J, Qi Y, Meng Z Y and Fu L 2017 *Phys. Rev. B* **95** 041101
[11] Huang L and Wang L 2017 *Phys. Rev. B* **95** 035105
[12] Shen H, Liu J and Fu L 2018 *Phys. Rev. B* **97** 205140
[13] Yu W, Liu Y, Chen Y, Jiang Y and Chen J Z Y 2019 *The Journal of Chemical Physics* **151** 031101
[14] Carleo G, Cirac I, Cranmer K, Daudet L, Schuld M, Tishby N, Vogt-Maranto L and Zdeborová L 2019 *Rev. Mod. Phys.* **91** 045002
[15] Mehta P, Bukov M, Wang C H, Day A G, Richardson C, Fisher C K and Schwab D J 2019 *Physics Reports* **810** 1
[16] Ackley D H, Hinton G E and Sejnowski T J 1985 *Cognitive Science* **9** 147
[17] Stratonovich R L 1957 *Soviet Physics Doklady* **2** 416
[18] Groshev A and Arzhnikov A 2020 *Journal of Experimental and Theoretical Physics* **130** 247
[19] Rrapaj E and Roggero A 2021 *Phys. Rev. E* **103** 013302
[20] Torlai G and Melko R G 2016 *Phys. Rev. B* **94** 165134
[21] Nomura Y, Darmawan A S, Yamaji Y and Imada M 2017 *Phys. Rev. B* **96** 205152
[22] Vieijra T, Casert C, Nys J, De Neve W, Haegeman J, Ryckebusch J and Verstraete F 2020 *Phys. Rev. Lett.* **124** 097201
[23] Carleo G and Troyer M 2017 *Science* **355** 602
[24] Hinton G E, Osindero S and Teh Y W 2006 *Neural Comput.* **18** 1527
[25] Morningstar A and Melko R G 2017 *J. Mach. Learn. Res.* **18** 5975 ISSN 1532-4435
[26] Azizi A and Pleimling M 2021 *Scientific Reports* **11** 1
[27] Ziman J and Ziman P 1979 *Models of Disorder: The Theoretical Physics of Homogeneously Disordered Systems* (Cambridge University Press) ISBN 9780521217842
[28] Binder K, Lebowitz J L, Phani M K and Kalos M H 1981 *Acta Metallurgica* **29** 1655
[29] Arzhnikov A, Bagrets A and Bagrets D 1996 *J. Magn. Magn. Mater.* **153** 195
[30] Müller M and Albe K 2005 *Phys. Rev. B* **72** 094203
[31] Cowley J M 1950 *Phys. Rev.* **77** 669
[32] Warren B E 1969 *X-ray Diffraction* (Addison-Wesley, Reading, MA)
[33] Scholten P D 1985 *Phys. Rev. B* **32** 345
[34] Newman M and Barkema G 1999 *Monte Carlo Methods in Statistical Physics* (Clarendon Press)
[35] Kawasaki K 1966 *Phys. Rev.* **145** 224
[36] Baxter R 1982 *Exactly Solved Models in Statistical Mechanics* (Academic Press)
[37] Binder K and Landau D P 1980 *Phys. Rev. B* **21** 1941
[38] Lourenço B J and Dickman R 2016 *J. Stat. Mech.: Theo. Exper.* **2016** 033107
[39] Arzhnikov A K, Dobysheva L V, Konygin G N, Voronina E V and Yelsukov E P 2001 *Phys. Rev. B* **65** 024419
[40] Kozak R, Sologubenko A and Steurer W 2015 *Zeitschrift für Kristallographie-Crystalline Materials* **230** 55
[41] Steurer W 2020 *Materials Characterization* **162** 110179
[42] Smolensky P 1986 *Parallel Distributed Process* **1**
[43] Hinton G E 2002 *Neural Computation* **14** 1771
[44] Hinton G E 2012 *A Practical Guide to Training Restricted Boltzmann Machines* (Berlin, Heidelberg: Springer) pp. 599–619
[45] Hyvärinen A 2006 *Neural Computation* **18** 2283
[46] Schönfeld B, Sax C R, Zemp J, Engelke M, Boesecke P, Kresse T, Boll T, Al-Kassab T, Peil O E and Ruban A V 2019 *Phys. Rev. B* **99** 014206